Excess Heat Capacity in Mo/Au Transition Edge Sensor Bolometric Detectors

Ari D. Brown, Regis P. Brekosky, Felipe Colazo-Petit, Matthew A. Greenhouse, James P. Hays-Wehle, Alexander S. Kutyrev, Vilem Mikula, Karwan Rostem, Edward J. Wollack, *Senior Member, IEEE*, and Samuel H. Moseley

***Abstract*—Excess heat capacity in a bolometric detector has the consequence of increasing or leading to multiple device time constants. The Mo/Au bilayer transition edge sensor (TES) bolometric detectors initially fabricated for the high resolution mid-infrared spectrometer (HIRMES) exhibited two response thermalization scales, one of which is a few times longer than estimates based upon the properties of the bulk materials employed in the design. The relative contribution of this settling time to the overall time response of the detectors is roughly proportional to the pixel area, which ranges between ∼0.3 and 2.6 mm^2. Use of laser ablation to remove sections of the silicon membranes comprising the pixels results in a detector response with a smaller contribution from the secondary time constant. Additional information about the nature of this excess heat capacity is gleaned from glancing incidence X-ray diffraction, which reveals the presence of molybdenum silicides near the silicon surface which is a consequence of the bi-layer deposition. Quantitative analysis of the concentration of excess molybdenum, estimated with secondary ion mass spectroscopy, is commensurate to the additional heat capacity needed to explain the anomalous time response of the detectors.**

***Index Terms*—Microfabrication, superconducting photodetectors, surface contamination, thin film sensors.**

I. Introduction

THE high resolution mid-infrared spectrometer (HIRMES) was slated to be a facility-class instrument for the Stratospheric Observatory for Infra-red Astrophysics (SOFIA). HIRMES was designed to probe several important aspects of protoplanetary formation by providing low (∼600) to very high (∼100000) spectroscopy in the 25–122 micron spectral regime [1].

Central to the HIRMES instrument were its two types of high filling fraction detector arrays [2], [3]: One was comprised of two 32×16 sub-arrays of 1 mm $\times$ 1 mm transition edge sensor (TES) pixels with a filling fraction of 84.7% in the spectral direction and 99.0% in the spatial direction, and the other was comprised of an 8×16 detector array of TES with eight rows of pixels of different dimensions for each row and a filling fraction ranging between 97.6% and 99.3% in the spatial direction for the smallest and largest pixels, respectively.

Two requirements for the latter, high resolution, detector pixels are a noise equivalent power (NEP) $\sim 3 \times 10^{-18}$ W/rt(Hz) and a response time ∼5 ms. With a simple thermal model [4], the effective response time of a TES bolometric detector $t_{eff} = t_0/(1+P\alpha/GT)$. Here P is the bias power of the voltage biased TES, and $\alpha = T/R\ dR/dT$, where T is temperature, R is the TES resistance. The natural time constant, $t_0 = C/G$, where C is the heat capacity and G is the thermal conductance between the TES and bath. Thus, in the absence of an excess heat capacity, the time response of a TES bolometer is linearly proportional to its heat capacity.

Initial development of the high resolution detectors for the HIRMES instrument involved their fabrication on low stress silicon nitride membranes. Detectors produced in early stages of HIRMES development employed silicon nitride membranes, which displayed much higher effective time constants (hundreds of ms) than anticipated from the nominal material parameters. An excess heat capacity associated with the as fabricated membrane structure was identified as the primary source of the observed response, however, the specific mechanism was not identified. A survey of the literature reveals examples of heat capacities in excess of the Debye model associated with silicon nitride films have been attributed to the presence of surface micro-states [5] and two-level systems [6] in previous low temperature work.

On account of the long time constants exhibited by the silicon nitride devices, a decision was made to abandon use of this material as a substrate. Subsequent detector development was undertaken on single crystal silicon substrates. Unexpectedly, these detectors also displayed much higher than anticipated time constants. In this manuscript, a discussion of possible sources and means to mitigate them are provided.

Manuscript received December 8, 2020; revised February 4, 2021; accepted March 7, 2021. Date of publication March 12, 2021; date of current version April 2, 2021. This work was supported by National Aeronautics and Space Administration, under Grant NNH15ZCA001N-S3GI. *(Corresponding author: Ari D. Brown.)*

Ari D. Brown, Matthew A. Greenhouse, and Edward J. Wollack are with the NASA Goddard Space Flight Center, Greenbelt, MD 20771 USA (e-mail: ari.d.brown@nasa.gov; matt.greenhouse@nasa.gov; edward.j.wollack@nasa.gov).

Regis P. Brekosky was with SSAI, Lanham, MD 20706 USA. He is now with NASA Goddard Space Flight Center, Greenbelt, MD 20771 USA (e-mail: regis.p.brekosky@nasa.gov).

Felipe Colazo-Petit is with the Teltrium Solutions, LLC, Rockville, MD 20852 USA (e-mail: felipe.a.colazopetit@nasa.gov).

James P. Hays-Wehle is with the University of Maryland, Baltimore, MD 21250 USA (e-mail: james.p.hays-wehle@nasa.gov).

Alexander S. Kutyrev is with the University of Maryland, College Park, MD 20742 USA (e-mail: alexander.s.kutyrev@nasa.gov).

Vilem Mikula is with American University, Washington, DC 20016 USA (e-mail: vilem.mikula-1@nasa.gov).

Karwan Rostem is with the University of Maryland, Baltimore, MD 21250 USA (e-mail: karwan.rostem@nasa.gov).

Samuel H. Moseley was with NASA Goddard Space Flight Center, Greenbelt, MD 20771 USA. He is now with Quantum Circuits, Inc., New Haven, CT 06511 USA (e-mail: harvey.moseley1@gmail.com).

Color versions of one or more figures in this article are available at https://doi.org/10.1109/TASC.2021.3065922.

Digital Object Identifier 10.1109/TASC.2021.3065922

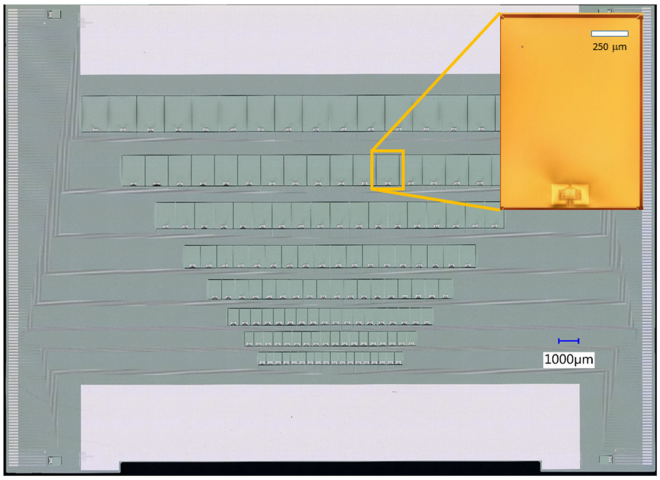

Fig. 1. Stitched micrograph of a HIRMES high resolution detector array.

II. HIRMES High Resolution Detectors

Fig. 1 shows a micrograph of a HIRMES high resolution detector array. There are eight 1 × 18 detector pixel arrays, in which the central 16 pixels of each array can be read out. The pixels are fabricated on 450 nm thick Si(001) substrates, which are suspended with 5 micron wide × 30 micron long thermal isolation structures. The TES are comprised of Mo/Au bilayer thin films, whose volume ∼1800 micron^3, with a superconducting transition temperature Tc∼110 mK and are read out via superconducting Nb leads. Additional components of the detector pixels include Ti/Au "heat-sinking" structures, with a volume ∼5600 micron^3 each, contacting the TES at two corners. These structures are used to engineer the pixel heat capacity, and NbTiN absorber coatings [7], [8], which coat the entire surface of the membrane on the side opposite the TES and which have AlN strain matching and Al_2O_3 stress compensating layers. Additional details regarding the fabrication of these detectors are provided in [3].

The largest pixels measure 1.40 mm × 1.84 mm and are, thus, ∼2.6 times larger than the largest leg-isolated single pixel silicon bolometers fabricated at NASA Goddard [9]. As discussed later in this manuscript, the contribution of bulk impurities distributed within the silicon membrane, coupled with a large pixel size, resulted in an excess heat capacity, which was several orders of magnitude greater than the Debye estimate of the silicon heat capacity.

III. Measurement of the Detector Temporal Response

The detector and time-domain multiplexing (TDM) chips were packaged and cooled in a cryogenic free system that reaches ∼70 mK using an adiabatic demagnetization refrigerator. Detector arrays were readout using TDM based upon superconducting quantum interference device (SQUID) electronics [10]. The detector signal was further amplified by a SQUID series array stage placed at 3K. The detector signal was sampled at a rate of 4167 Hz. A square waveform with a 2 second period was added to the DC TES bias signal to excite the electrothermal circuit and measure the pixel response functions. The amplitude of the square wave is less than 0.05% of the DC bias value. Examples of the measured detector temporal response are shown in Fig. 2(b) and (d).

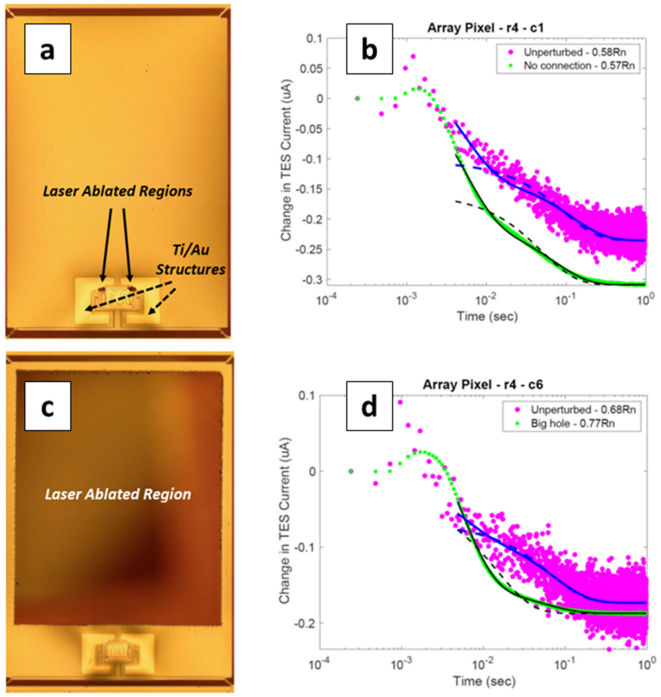

Fig. 2. (a) Image of a detector pixel, in which the Ti/Au heat-sinking structure/TES overlap regions were laser ablated. (b) Time response of the pixel after laser ablation (green curve), illustrates that the decay curves are qualitatively similar. The dashed and solid lines represent single and double exponential decay fits, respectively. In the case of the double exponential decay fit, one of the time constants = 5 ms. (c) Image of a detector pixel in which the central region of the detector pixel has been laser ablated. (d) Removal of this region makes a substantial impact to the detector speed: The ratio of the weight of the fast time constant and the slow one is 3.6 for the ablated pixel and only 0.3 for the unperturbed one. In both (a) and (c), the pixel dimensions are 0.68 mm × 0.98 mm. Note that in both (b) and (d), the time response data shown for the laser ablated pixels were averaged over multiple pulses.

IV. Identification of a Root Cause and Mitigation Approaches

From the measurements taken and described in Section III, it was hypothesized that the root cause of the additional time constant was a dangling heat capacity [11]. Some possible sources of this dangling heat capacity were either: (1) The Ti/Au heat-sinking structures, which may have been thermally decoupled to the TES on account of a superconducting Nb joint, or, (2) one or more layers of surface contamination.

In order to evaluate the contribution of the former, we laser ablated the Ti/Au heat-sinking structure – TES *overlap region* on some pixels, shown in Fig. 2(a), and removed both of the Ti/Au heat-sinking structures and the underlying silicon membranes on others. Fig. 2(b) shows the time response of a pixels in which the overlap region was laser ablated. The time response of the modified pixel, which has a second pole and is shown in green, is largely unchanged relative to that on another, unmodified, pixel with the same surface area. A similar effect is seen on pixels, which had both of the Ti/Au structures as well as the

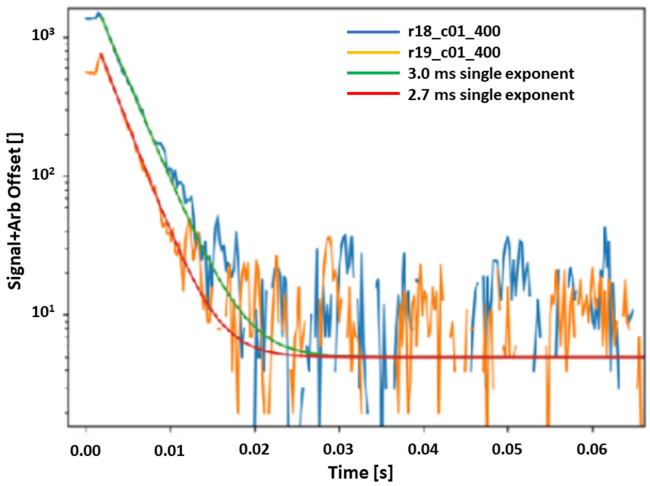

Fig. 3. Time response of two detector pixels after the top 10 nm of silicon substrate had been, inadvertently, been etched. Note the presence of a single pole response.

underlying silicon substrate removed; whereas the first, natural time constant is smaller in these cases, the weight of the second time constant was not appreciably impacted. As an aside, it is worth noting that the superconducting transition temperature, saturation power, and transition shape were unaltered by laser ablating regions only tens of microns away from it.

We further exploited the ability to laser ablate regions to identify the location of the dangling heat capacity on the pixels. One modification to certain pixels consisted of ablating regions near the pixel perimeter. This modification resulted in no appreciable change to the detector's time response, and was in disagreement with one hypothesis, in which condensation of fluoropolymers formed during the reactive ion etching process, used to define the membranes, contributed to excess heat capacity.

Another modification consisted of ablating the central portion of the pixel, in which 73% of the membrane was removed (see Fig. 2(c) and (d)). This modification resulted in a sharp decrease in the weight of the second time constant. Thus, it was inferred that the source of the excess heat capacity resided either on the silicon surface or within its bulk.

In order to look for the presence of surface contamination, scanning electron microscopy (SEM) was performed. Conventional electron microscopy, using an electron voltage of 10 kV, did not reveal any contamination. However, by using low voltage electron microscopy, with voltage $<$5 keV, a layer of residue resided near the perimeter of some pixels was observed. Because this residue could not be imaged at higher voltage, it was believed that the residue was organic in nature. This led to the application of a cleaning process demonstrated to remove organic residues on the detector pixels. This process consisted of a succession of intense UV-light exposure, immersion in a commercially available organic base, and oxygen plasma ashing in a reactive ion etcher. After cleaning the pixels, the residues could no longer be seen in the SEM. Furthermore, and more importantly, the amplitude and time constant of the second component was reduced by a factor of four.

The cleaning process reduced a substantial fraction of the dangling heat capacity; however, it did not fully eliminate it. This suggested that there were contaminants inside the silicon bulk. Regions near the surface of the silicon membrane were probed with glancing incidence X-ray diffraction. Using an incidence angle $\sim$0.2°, which corresponds to an X-ray penetration depth of $\sim$7 nm in silicon [12], evidence of the presence of a molybdenum silicide, Mo_5Si_3, was seen. This result was unexpected, because the estimated amount of interdiffusion between Mo and Si after the Mo was deposited is $<$1 nm [13]. Thus, athermal mechanisms may have contributed to implantation of sputtered Mo atoms into the single crystal silicon substrate.

In order to quantify the amount of the molybdenum contaminant in the silicon bulk, secondary ion mass spectroscopy (SIMS) was performed. Although the SIMS cannot accurately provide atomic concentration as a function of depth into the bulk, because of resputtering of the sample's constituent atoms, one can obtain an accurate value of the areal concentration by integrating the volume concentration over the sample thickness.

The impact of molybdenum contaminants upon the pixel time response can be inferred by integrating the SIMS-obtained concentration profiles to obtain the molybdenum areal concentration $= 1.8 \times 10^{15}$ atoms/cm^2. For the largest HIRMES pixels, the resulting excess heat capacity $\sim$1.4 pJ/K at 0.1 K [14]. This value is approximately 17 times larger than that derived from all the pixel components. Furthermore, the magnitude of the heat capacity contribution from the excess molybdenum is similar to that extracted from $G \times t_0$. For the fifth-largest pixels, whose dimensions $=$ 0.82 mm $\times$ 1.14 mm, the estimated Mo contribution to heat capacity is 0.5 pJ/K at 0.1 K. This value is the same, within error, as $G \times t_0$.

Evidence that the second time constant is associated with the presence of molybdenum silicide is found in two pixels, in which the top $\sim$10 nm of silicon absorber membrane surface had been, inadvertently, ion milled. After this modification their time response exhibited a single exponential decay, t_{eff} $\sim$2.85 ms.

These observations are consistent with the molybdenum contaminants near surface regions of the silicon membranes as being a major contributor to an excess, dangling, heat capacity. Some methods to mitigate or eliminate the presence of the molybdenum contaminants might include the use of a lower power Mo sputtering deposition process, depositing the Mo in another manner [15], depositing the Mo through a lift-off mask, or employing a low heat capacity diffusion barrier.

V. Conclusion

High filling fraction TES bolometric detector pixels with Mo/Au TES bilayers deposited on crystalline silicon substrates were found to have two time constants, one of which was much larger than the other and whose weight scaled with pixel area. We attribute this additional time constant to a dangling heat capacity, which takes the form of organic residue and molybdenum atoms embedded in the silicon membrane. We have demonstrated fabrication methodologies to remove both of these contaminants, and future large area and high filling factor bolometric detectors with millisecond time constants may need to follow these methodologies in order to achieve their expected performance.

Acknowledgment

The SIMS characterization of our samples was provided by Eurofins EAG Materials Science.

REFERENCES

[1] S. N. Richards *et al.*, "SOFIA-HIRMES: Looking forward to the HIgh-Resolution Mid-infrared spectrometer," *J. Astronom. Instru.*, vol. 7, no. 4, 2018, Art. no. 1840015.

[2] E. M. Barrentine *et al.*, "Characterization of Si membrane TES bolometer arrays for the HIRMES instrument," *J. Low Temp. Phys.*, vol. 193, p. 241, 2018, https://doi.org/10.1007/s10909-018-1966-4.

[3] A. D. Brown *et al.*, "Fabrication of ultrasensitive TES bolometric detectors for HIRMES," *J. Low Temp. Phys.*, vol. 193, p. 675, 2018, https://doi.org/10.1007/s10909-018-1914-3.

[4] K. D. Irwin, "An application of electrothermal feedback for high resolution cryogenic particle detection," *Appl. Phys. Lett.*, vol. 66, p. 1998, 1995, https://doi.org/10.1063/1.113674.

[5] M. Kenyon, P. K. Day, C. M. Bradford, J. J. Bock, and H. G. Leduc, "Heat capacity of absorbers for transition edge sensors suitable for space-borne Far-IR/Submm spectroscopy," *IEEE Trans. Appl. Supercond.*, vol. 19, no. 3, pp. 524–527, Jun. 2009.

[6] M. E. Eckart *et al.*, "Experimental results and modeling of low-heat-capacity TES microcalorimeters for soft-X-ray spectroscopy," *AIP Conf. Proc.*, vol. 1185, p. 430, 2009, https://doi.org/10.1063/1.3292370.

[7] T. M. Miller *et al.*, "A path to high-efficiency optical coupling for HIRMES," *J. Low Temp. Phys.*, vol. 193, p. 681, 2018, https://doi.org/10.1007/s10909-018-1939-7.

[8] A. D. Brown, K. H. Miller, and W. J. Wollack, "Niobium titanium nitride thin film coatings for far-infrared absorption and filtering," U.S. Patent 10458853, 2019.

[9] D. Benford *et al.*, "5,120 superconducting bolometers for the PIPER balloon-borne CMB polarization experiment," *Proc. SPIE*, vol. 7741, 2010, Art. no. 77411Q.

[10] W. B. Doriese *et al.*, "Developments in time-division multiplexing of X-ray transition-edge sensors," *J. Low Temp. Phys.*, vol. 184, pp. 389–395, 2016, https://doi.org/10.1007/s10909-015-1373-z.

[11] I. Maasilta, "Complex impedance, responsivity, and noise of transition edge sensors: Analytical solutions for two- and three-block thermal models," *AIP Adv.*, vol. 2, 2012, Art. no. 042110.

[12] K. Omote, "High resolution grazing-incidence in-plane X-ray diffraction for measuring the strain of a Si thin layer," *J. Phys. Condens. Matter.*, vol. 22, 2010, Art. no. 474004. doi:10.1088/0953-8984/22/47/474004.

[13] K. Holloway, K. B. Do, and R. Sinclair, "Interfacial reactions on annealing molybdenum-silicon multilayers," *J. Appl. Phys.*, vol. 65, p. 474, 1989.

[14] G. R. Stewart, "Measurement of low-temperature specific heat," *Rev. Sci. Instru.*, vol. 54, pp. 1, 1983, https://doi.org/10.1063/1.1137207.

[15] F. M. Finkbeiner *et al.*, "Electron-beam deposition of superconducting molybdenum thin films for the development of Mo/Au TES X-ray microcalorimeters," *IEEE Trans. Appl. Supercond.*, vol. 27, no. 4, Jun. 2017, Art. no. 2100104.